

DRAG FORCE ON BUBBLES IN BUBBLE SWARMS

Ivo Roghair*, Martin van Sint Annaland and Hans Kuipers

Fundamentals of Chemical Reaction Engineering (FCRE)
 Institute of Mechanics, Processes and Control-Twente (IMPACT),
 University of Twente, Enschede, The Netherlands

* Corresponding author, E-mail address: i.roghair@tnw.utwente.nl

ABSTRACT

Direct Numerical Simulations with a Front Tracking model have been used to study the hydrodynamic behavior of bubble swarms for the air/water system. In this work, we focus on the effect of the presence of neighboring bubbles on the drag as a function of the void fraction, especially at higher void fractions. Mimicking bubble swarms with a relatively small number of bubbles in a periodic domain, the number of bubbles was varied while keeping the overall void fraction constant. We have observed a strong hindered rise effect, while bubbles tend to arrange themselves in horizontal clusters. The observed minimum in the drag coefficient as a function of the number of bubbles at a fixed void fraction was related to the maximum number of bubbles that can coordinate themselves in a horizontal plane.

The normalized drag coefficient increases for higher void fractions (i.e. hindered rise). Again, significant effects of horizontal bubble clustering on the drag coefficient were found and explained.

NOMENCLATURE

See also Table 1 or text near the relevant equations.

A	Projected surface area
C_D	Drag coefficient
E	Aspect ratio
F_B	Buoyancy force
F_D	Drag force
F_σ	Surface tension force
g	Gravitational constant
L	Length of computational domain
n_{\max}	Max. number of bubbles in a plane
\mathbf{n}	Normal vector
p	Pressure
S	Surface area
\mathbf{t}_{ma}	Tangent between markers m and a
v_z	Bubble rise velocity
V	Volume
\mathbf{u}	Velocity vector
$\boldsymbol{\tau}$	Stress tensor
σ	Surface tension coefficient
ϕ	Packing density

Subscripts

c	Continuous (liquid) phase
d	Dispersed (bubble) phase
$glob$	Global
rel	Relative
z	Vertical direction
∞	Single bubble in an infinite liquid

INTRODUCTION

Bubble columns are frequently applied in the metallurgical and (bio)chemical process industries as an efficient gas-liquid contacting device. In reactive systems, the contact area between the gas and liquid phases is of major importance for efficient process operation, while in mixing applications (e.g. the stirring of liquid steel by means of gas bubbles) the overall hydrodynamic flow pattern is of specific interest. The modelling of bubble columns requires CFD simulations, using real process length scales to cover the entire bubble column unit. Of course, these large scale models cannot resolve the smallest details of the flow, but can provide important information on the macroscopic circulation patterns and void fraction profiles in relatively short calculation times, provided that the details of the interaction between the phases is modelled with accurate closure correlations. Deriving such correlations with more detailed types of models that can capture these specific, detailed phenomena is what we refer to as a multi-level modelling approach (a.o. Deen *et al.*, 2004).

The drag force is the most important force acting on bubbles in a bubble column, since it dominantly controls the rise velocity of the bubbles through the liquid, determining the gas phase residence time and driving the macroscopic flow patterns. An accurate description of the drag coefficient C_D as a function of the Reynolds number is essential for Discrete Element Methods, which simulate bubbly flow in an Euler-Lagrangian manner up to $O(10^6)$ bubbles, or Multi-Fluid Models that treat both phases as interpenetrating continua. It is therefore not surprising that numerous drag force closures can be found in literature. A distinction has to be made between closures that describe the drag coefficient of single bubbles in an 'infinite' quiescent liquid, e.g. Tomiyama *et al.* (1998) and Mei *et al.* (1994), and other relations describing the drag force on bubbles in a swarm, e.g. Simonnet *et al.* (2007).

Bubble swarms

Drag correlations for bubble swarms can be derived from simulations or experiments, and are mainly described as a function of the Reynolds number Re , the Eötvös number Eu and the void fraction (gas phase fraction) α . The effect of the local void fraction on the drag coefficient is often accounted for via a correction of the terminal rise velocity via:

$$v_z = v_\infty (1 - \alpha)^n \quad (1)$$

Where v_∞ is the rise velocity of a single bubble in an infinite liquid, and n is often called the Richardson-Zaki exponent (Richardson & Zaki, 1954). A particular modification of this

correlation, derived experimentally for gas-phase fractions up to 50%, is that of Lockett & Kirkpatrick (1975) (Eq. 2).

$$V_{\text{rel}} = V_{\infty} (1 - \alpha_{\text{glob}})^{1.39} \times (1 + 2.55\alpha_{\text{glob}})^3 \quad (2)$$

A further outline of existing correlations of this form has been given in the work of Simonnet *et al.* (2007), who have also measured the rise velocity of bubbles in a swarm experimentally for the air/water system. They have found bubble hindrance up to a void fraction of about 15% (increased drag coefficient), whereas beyond a void fraction of 15%, the bubbles showed cooperative rise (reduced drag compared to a single bubble in an infinite liquid).

Results of direct numerical simulations of bubble swarms have also been reported in the literature, for instance the work of Bunner & Tryggvason (2002). They have comprehensively described their results of bubble swarm simulations using relatively large numbers of bubbles (up to 216 bubbles) with their Front Tracking model. However, they concluded that the interactions between bubbles could already be found using only 12 bubbles in a periodic domain, and found that bubbles tend to cluster horizontally and vertically, the latter referred to as ‘‘acceleration, kissing and tumbling’’. Bunner & Tryggvason (2002) simulated bubble swarms using a density ratio ρ_d/ρ_c and viscosity ratio μ_d/μ_c of 1/50 to avoid numerical instabilities, so that their bubbles were mainly spherical or slightly ellipsoidal shaped. These numerical problems, for example the high density jump between the phases, can be overcome by more sophisticated algorithms to handle the pressure jump at the interface (e.g. Francois *et al.* (2006); Dijkhuizen (2008)), opening up the possibility to simulate air bubble swarms in water.

In this work, we study the drag force of air bubble swarms in water at relatively high void fractions by simulating a small number of bubbles in a periodic domain. First, the Front Tracking model is shortly introduced. Subsequently, we study the influence of the selected number of bubbles in a periodic domain while keeping the void fraction the same, and show how the number of bubbles affects the bubble clustering and drag coefficient. Finally, we describe the drag coefficient as a function of the void fraction.

FRONT TRACKING MODEL

Front Tracking modelling is a well-known Direct Numerical Simulations (DNS) method (a.o. Unverdi & Tryggvason, 1992; van Sint Annaland *et al.*, 2006; Dijkhuizen, 2008) to simulate multiphase flows with deformable interfaces in full detail. The main advantage of Front Tracking modelling for this work is that bubbles do not coalesce unless a specific merge condition is implemented (see e.g. Singh & Shyy (2007)). A short introduction of the Front Tracking method employed in this work is given here. For a more detailed description, and a validation for the drag on single rising bubbles, see Dijkhuizen (2008).

Flow solver

The fluid flow is described with a single fluid formulation of the Navier-Stokes equation for incompressible fluids (Eq. 3), while mass conservation is enforced by the continuity equation (Eq. 4):

$$\rho \frac{\partial \mathbf{u}}{\partial t} = -\nabla p - \rho \nabla \cdot (\mathbf{u}\mathbf{u}) - \nabla \cdot \boldsymbol{\tau} + \rho \mathbf{g} + \mathbf{F}_{\sigma} \quad (3)$$

$$\nabla \cdot \mathbf{u} = 0 \quad (4)$$

where \mathbf{u} is the fluid velocity, $\boldsymbol{\tau}$ the stress tensor and p the pressure. We use a finite difference technique on a staggered grid and solve the discretized equations using a standard two-stage projection-correction method with an efficient ICCG matrix solver.

Interface mesh

The interface between the phases is tracked using Lagrangian control points. The interconnection between these points form a mesh of triangular markers. In Eq. 3, \mathbf{F}_{σ} accounts for the surface tension force, that can be directly evaluated from the markers’ positions. The individual pull-force of marker a acting on marker m can be computed from their normal vectors and joint tangent:

$$\mathbf{F}_{\sigma, a \rightarrow m} = \sigma (\mathbf{t}_{ma} \times \mathbf{n}_a) \quad (5)$$

The total surface tension force on a marker is thus obtained by using Eq. 5 on all three neighboring markers of m . The surface tension force is \mathbf{F}_{σ} is then mapped to the Eulerian cells closest to marker m , using mass-weighting (Deen *et al.*, 2004).

An infamous aspect of DNS for very small bubbles (e.g. 1 mm air bubble in water) is the treatment of the large pressure jump at the gas-liquid interface, which may cause spurious or parasitic currents that affect the final solution significantly. Similar to the techniques developed by Renardy & Renardy (2002) and Francois *et al.* (2006) for Volume Of Fluid (VOF) methods, the pressure jump has been accounted for in the following manner:

$$[p] = \frac{\int_{\partial S} [p] dS}{\int_{\partial S} dS} = \frac{\int_{\partial S} \mathbf{F}_{\sigma} \cdot \mathbf{n}}{\int_{\partial S} dS} = \frac{\sum_m \mathbf{F}_{\sigma, m} \cdot \mathbf{n}_m}{\sum_m S_m} \quad (6)$$

When the surface tension force over all the markers has been calculated, the pressure jump over the interface can be computed and subsequently be mapped back to the interface control points. This method of treating the pressure jump reduces the parasitic currents for the 1 mm air bubble in water case with two orders of magnitude, compared to Front Tracking models without this implementation (Dijkhuizen, 2008).

After computation of the fluid flow, the Lagrangian control points are moved to their new locations at every time step. The fluid flow is interpolated using cubic splines, which are constructed from the region around each bubble separately. The presence of other bubbles within this region, does not affect the construction of the splines, because the flow field is continuous over the interface. The markers are advected with the interpolated fluid flow using 4th order Runge-Kutta time stepping.

The phase fraction is derived from the marker position analytically using an efficient DTA (Divergence Theorem Algorithm). The density in each Eulerian cell is calculated by weighted averaging with the phase fraction, while the viscosity is obtained by weighted harmonic averaging of the kinematic viscosities (Prosperetti, 2002).

Adaptive time stepping

Computationally efficient simulation of dense bubble swarms requires an Adaptive Time Stepping (ATS) technique. Especially when bubbles approach each other

closely, the flow needs to be resolved with a much higher temporal resolution than, for instance, a single bubble case. A simple, but efficient, ATS scheme was implemented, following the work by Alexander (1977).

For every time step the solution at the next time step is calculated twice; first using a single full time step from t to $t + \Delta t$, and then twice using a time step of $\frac{\Delta t}{2}$. The results of these two calculations are compared. If the difference between the solutions for Δt and $2\frac{\Delta t}{2}$ exceeds a predefined threshold, the timestep is decreased with 20%. If the difference is very small, the timestep is enlarged with 20%.

NUMERICAL SIMULATIONS

Numerical simulations of monodisperse bubble swarms were performed using the physical properties for air bubbles in water. The properties and numerical settings can be found in Table 1. The computational domain was chosen cubic at all times, with full 3D periodic boundary conditions. The Eulerian cell size was set such that 20 grid cells fit on an equivalent bubble diameter at the start of the simulations. The typical simulation settings are based on grid/time step dependency tests (a.o. Dijkhuizen, 2008; Hua *et al.*, 2008). The void fraction was adjusted by increasing or decreasing the domain size. Initially, the bubbles are

Property	Symbol	Value
Bubble diameter	d	2 – 6 mm
Number of bubbles	n_{bub}	1 – 16
Gas phase fraction	α	1 – 42 %
Mesh width	Δx	$\frac{d}{20}$
Domain size	n_x, n_y, n_z	Varies with α
Marker size (remeshing)		0.2 to 0.4 Δx
Time step	Δt	$10^{-7} - 2 \cdot 10^{-4}$
Simulation time	t_{end}	0.5 – 3.0 s
Gas density	ρ_d	1.25 kg m^{-3}
Gas viscosity	μ_d	$1.8 \cdot 10^{-5} \text{ Pa s}$
Liquid density	ρ_c	1000 kg m^{-3}
Liquid viscosity	μ_c	10^{-3} Pa s
Surface tension coefficient	σ	0.073 N m^{-1}

Table 1: General numerical settings for the air-water bubble swarm simulations.

spherical and placed randomly through the domain. Their initial positions were calculated with a Monte-Carlo simulation (Frenkel & Smit, 2002); starting with an ordered configuration, the Monte-Carlo procedure perturbs the position of the bubbles in a random fashion and determines the amount of overlap between bubbles after each move. If the overlap is too large, the move is rejected, otherwise it is accepted. This procedure includes support for periodic boundary conditions. The final step in this procedure does not allow any overlap between bubbles.

The drag coefficient C_D is obtained from the force balance on a bubble, when the buoyancy is exactly counteracted by the drag force, resulting in Eq. 7.

$$\begin{aligned}
 0 &= F_B + F_D \\
 0 &= V(\rho_c - \rho_d)g_z - C_D A \frac{\rho_c}{2} |v_z - u_z| (v_z - u_z) \\
 C_D &= \frac{4d(\rho_c - \rho_d)g_z}{3\rho_c \langle (v_z - u_z)^2 \rangle} \quad (7)
 \end{aligned}$$

n_{bub}	d	Slip vel. [m/s]	Std. dev.
1	2 mm	0.255	—
2	2 mm	0.163	$7.3 \cdot 10^{-04}$
4	2 mm	0.137	$5.1 \cdot 10^{-03}$
8	2 mm	0.138	$1.2 \cdot 10^{-02}$
16	2 mm	0.173	$1.4 \cdot 10^{-02}$
32	2 mm	0.171	$3.5 \cdot 10^{-02}$
1	4 mm	0.210	—
2	4 mm	0.158	$3.7 \cdot 10^{-04}$
4	4 mm	0.174	$2.0 \cdot 10^{-02}$
8	4 mm	0.179	$1.3 \cdot 10^{-02}$
16	4 mm	0.192	$1.4 \cdot 10^{-02}$

Table 2: Slip velocities of $d = 2$ mm and $d = 4$ mm cases, for 2, 4 and 8 bubbles in a periodic box at 12% gas phase fraction. The standard deviation of the average velocity of all bubbles in the domain is also shown.

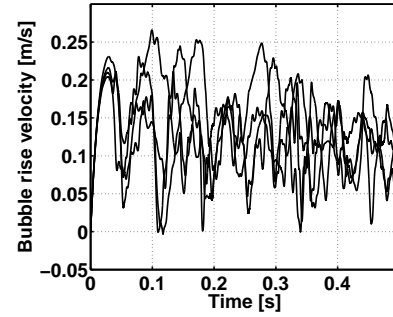


Figure 1: The rise velocity of four $d = 2$ mm bubbles in a periodic domain. The gas phase fraction is 12%. The bubbles show interaction with each other already after about 0.05s. (Not the entire simulation time has been shown for clarity.)

We calculate C_D using the time average slip velocity of the bubble and the liquid. The drag coefficients obtained for multiple bubbles in a simulation are then averaged over all bubbles in the domain. This method is preferred, since the slip velocity of bubbles is sometimes zero (due to tumbling effects), and the C_D will go to infinity.

RESULTS

Number of bubbles

In this section the effects of the number of bubbles in a periodic box are investigated at the same void fraction, varying between 1 and 16 bubbles (and a preliminary result for 32 bubbles). First, the time-averaged bubble rise velocity is determined for all bubbles from the simulation results, and the average velocity of the liquid in the domain is subtracted, yielding the average bubble slip velocity (see Table 2). Of course, initial effects have to be disregarded, but these effects disappear rather quickly (depending on the void fraction, but typically within 0.2 s; see Figure 1 for an example of the slip velocity of four bubbles with $d = 2$ mm). The standard deviation in the time-averaged, number-averaged slip velocity is very high and amounts to about 10% of the average velocity, which can also be observed from the wide spread of slip velocities of the different bubbles in Figure 1.

While keeping the void fraction fixed at 12%, the average slip velocity shows a minimum as a function of the selected number of bubbles in the computational domain, both for

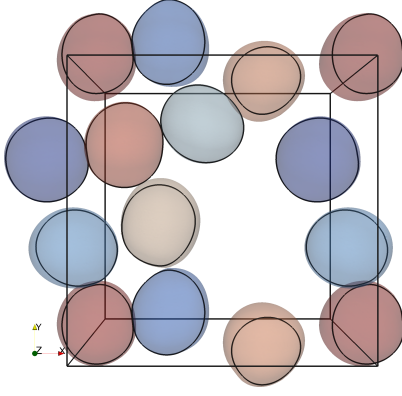


Figure 2: A top-down view of an 8-bubble simulation ($d = 2$ mm) with a void fraction of 12% showing the horizontal alignment of the bubbles. The black circumferencing lines on the bubbles show the bubble surface cross-section at the horizontal plane centered vertically in the domain. The color filled areas show the entire vertically projected area of the bubbles.

the case of 2 and 4 mm bubbles. This effect also has been observed by Bunner & Tryggvason (2002) using simulations with 4 and 12 bubbles at 6% void fraction. The explanation of this effect is the horizontal coordination of the bubbles in a plane. A cut-plane perpendicular to the vertical axis (i.e. the vertically projected area) shows that the bubbles align preferably horizontally (Figure 2). The maximum number of bubbles that can align in a horizontal plane n_{\max} can be calculated as a function of the total number of bubbles n_b , the (locally averaged) void fraction α , the bubble aspect ratio $E = d_z / \sqrt{d_x d_y}$ and the maximum horizontal packing fraction ϕ_{\max} , assuming a cubic computational domain is given by:

$$n_{\max} = \frac{4\phi}{\pi} \left(\frac{n_b \pi E}{6\alpha} \right)^{\frac{2}{3}} \quad (8)$$

The averaged bubble aspect ratio E can be obtained directly from the simulation output (summarized in Figure 3a), whereas the number of bubbles and the void fraction were input for the simulations. The maximum packing fraction of monodisperse solid disks (ellipses or circles) in a horizontal plane is known to be at maximum $\phi = \frac{\pi}{\sqrt{12}} \approx 0.9069$. However, for a randomly packed state of circles this is about $\phi \approx 0.82$ (Kausch *et al.*, 1971). For our case with deformable rising bubbles through a liquid the maximum bubble fraction of bubbles is even lower, and we estimate the maximum “packing” fraction of the bubbles in a horizontal plane to be approximately $\phi_{\max} = 0.7$. The ratio of the number of bubbles in the cubic domain relative to the maximum number of bubbles in a horizontal plane is given by Figure 3b as a function of the selected number of bubbles for 2 mm and 4 mm bubbles.

Case with 2 mm bubbles

A closer investigation of the strong increase in slip velocity for the cases with $n_b = 8$ and $n_b = 16$ is carried out (see Table 2). The aspect ratio E of the 2 mm bubbles is about 0.9 as can be discerned from Figure 3a. Using Eq. 8, it is found for $\alpha = 12\%$ that $n_b/n_{\max} \geq 1$ for 12 bubbles or more, which indicates that, in our cubic domain, maximally 12 bubbles can cluster horizontally when the void fraction is set to 12%. A larger number of bubbles will cause the “excess” bubbles to form a separate plane or to move freely

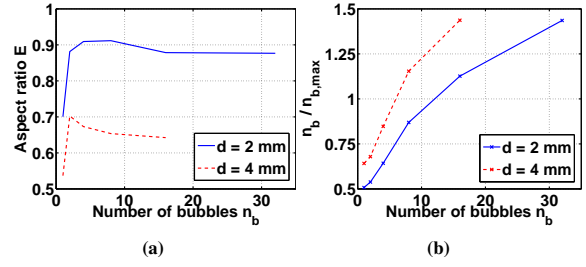


Figure 3: The aspect ratio (a) and n_b/n_{\max} (b) as a function of the selected number of bubbles for the 2 and 4 mm cases. Notice that the lower aspect ratio of the 4 mm bubbles n_b/n_{\max} to increase faster than for more spherical, 2 mm bubbles.

between the (periodic) planes. This is illustrated in Figure 4, where snapshots of the simulation results with a different number of bubbles are shown. For the $n_b = 8$ case, the bubbles are found preferentially on the same height in the domain, whereas the $n_b = 16$ case shows many bubbles crossing between planes, which are accelerated by the wakes of the leading bubbles, thus increasing their rise velocity.

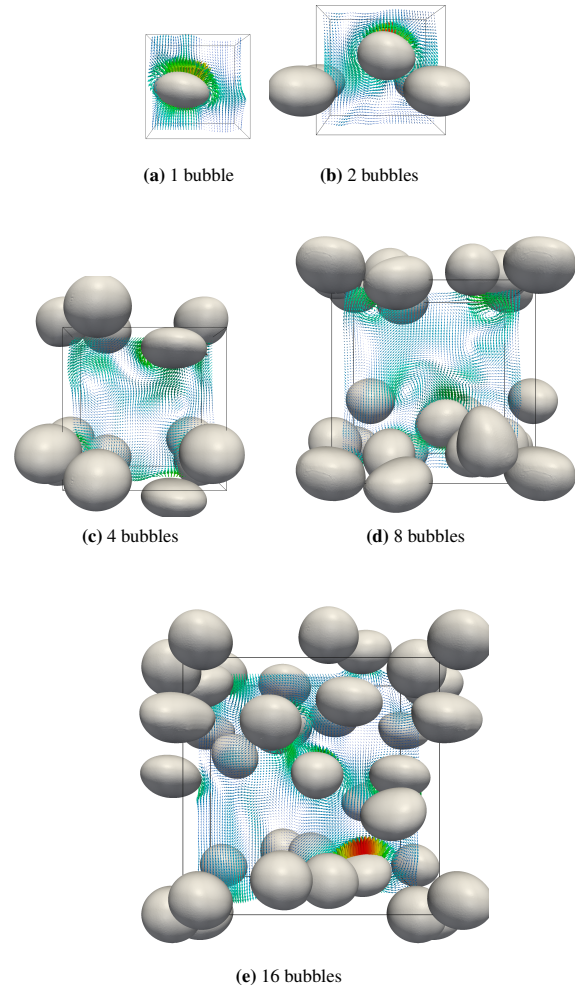


Figure 4: Snapshots of simulations with a different number of bubbles in a cubic domain with a fixed void fraction of $\sim 12\%$. (Air bubbles in water with an equivalent diameter $d = 2$ mm. Images are printed to relative scale.)

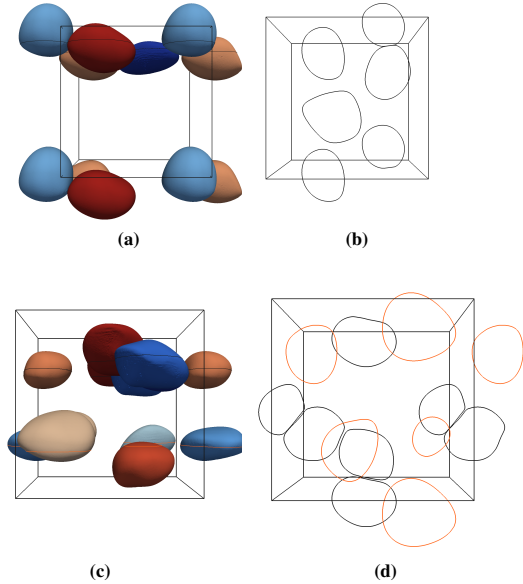


Figure 5: Horizontal bubble clustering for $n_b = 4$ and $n_b = 8$ cases ($d = 4$ mm). The maximum number of bubbles that fit in a plane is approximately 6, so in the first case, all bubbles in the domain prefer to align horizontally with all the other bubbles. In the second case, the bubbles distribute over 2 planes with each 4 bubbles.

Case with 4 mm bubbles

Bubbles with a diameter $d = 4$ mm in a bubble swarm (air/water system) are much more oblate ($E \approx 0.65$), as can be deduced from Figure 3a. As a result of the larger vertically projected area of the bubbles, fewer bubbles fit maximally in a horizontal plane ($n_b/n_{\max} \approx 1$ at $n_b = 6$). With four bubbles in the domain, a preference to align in a single plane is observed (Figure 5a–5b). With eight bubbles, two planes are occasionally formed, and the bubbles in the domain are distributed over these two horizontal planes (Figure 5c–5d).

Drag force in swarms

The drag force of swarms with 8 air bubbles with $d = 4$ mm in water is obtained as a function of the void fraction. The void fraction is varied by changing the domain size, so that $1.6\% \leq \alpha \leq 34.8\%$ using 11 different values for α . Larger numbers of bubbles (i.e. $n_b \geq 16$ bubbles in a periodic domain) could only be performed at high gas fractions (since the computational domain increases with decreasing void fraction) and hence do not provide insight of the drag coefficient at lower void fractions.

Figure 6 shows the normalized drag coefficient (i.e. relative to the drag coefficient of a single bubble rising in an infinite, initially quiescent liquid) as a function of the void fraction. We compare our results with the correlation of Lockett & Kirkpatrick (1975), i.e. Eq. 2, from which a C_D was derived. Although both simulations and experiments show a rising trend as a function of the gas phase fraction, it is clear that our simulations predict a higher normalized drag coefficient for bubbles in a swarm. Because the measurements on which this correlation is based were carried out with tap water, the discrepancy may be (partly) attributed to the effect of contaminants. Moreover, large-scale circulation patterns do not develop in the periodic domain in our simulations, whereas it could have influenced the experimental results.

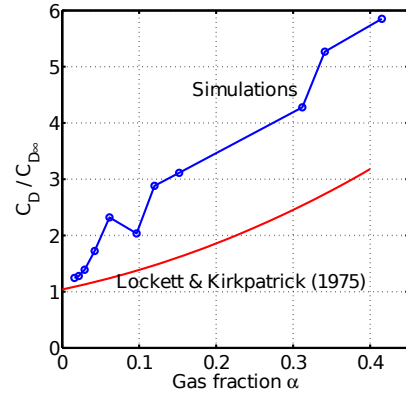


Figure 6: The normalized drag coefficient $C_D/C_{D,\infty}$ on 8×4 mm bubbles, as a function of the void fraction α shows an increase at higher gas hold-ups. The errorbars show the standard deviation of the different drag coefficients obtained for the 8 bubbles.

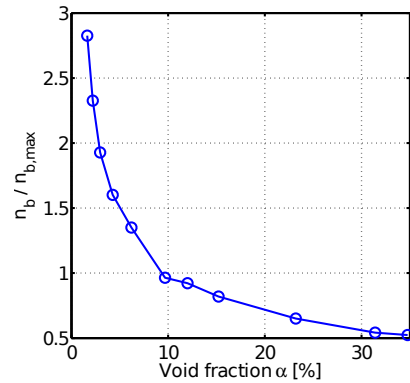


Figure 7: The maximum number of bubbles that can form a horizontal plane in the periodic box is plotted as a function of the number of bubbles that could be used. In our simulations we have used 8 bubbles. We find $n_b = n_{\max}$ for the simulation with 9.7%.

On the other hand, 8 bubbles in a domain could also not be sufficient to capture all bubble interactions. Due to computational restrictions, it is not yet possible to simulate large numbers of bubbles at different void fractions for a sufficiently long time.

In general, we found that the slip velocity of the bubbles only decreases as the void fraction increases (i.e. hindered rise). The small dip at a void fraction of about 9.7% deviates from the general trend and raised particular interest. Inspecting the individual bubble tracks of this particular simulation, we found that bubble tumbling did hardly occur in this simulation, whereas this is a commonly observed phenomenon in the other simulations. Tumbling occurs when bubbles rise through a plane of bubbles and collide with them (the “kissing” step). Due to the tumbling that follows, the bubbles are slowed down, or even show negative slip velocities (see Figure 1). However, this does not happen for the 9.7% simulation. Equation 8 is evaluated for the simulations performed in this section, to investigate plane-formation effects. The value of n_{\max} is very close to 1 for the simulation with a 9.7% void fraction (see Figure 7). Hence, for this particular case all the bubbles in the domain just fit on a single horizontal plane, and the bubbles hardly cross over between the (periodic) planes. This illustrates that horizontal bubble clustering strongly affects the drag coefficient, and may

need to be taken into account in drag closure correlations. Finally, we do not observe a decreasing drag coefficient (i.e. cooperative rise) beyond about 15% void fraction, as measured by Simonnet *et al.* (2007). These discrepancies might be related to the macroscopic circulation patterns in actual bubble columns.

CONCLUSIONS

We have investigated the hydrodynamic behavior of bubble swarms for the air/water system using Front Tracking simulations, using periodic boundary conditions to mimic large bubble swarms.

First we evaluated the influence of the selected number of bubbles on the time-averaged and number-averaged drag coefficient, while keeping the void fraction and other physical parameters constant. Hindered rise with a minimum in the drag coefficient as a function of the number of bubbles was found, which is related to the preferential horizontal alignment of the bubbles.

Subsequently, the drag coefficient as a function of the void fraction was studied using 8 air bubbles in water in a periodic domain by varying the computational domain size. The drag coefficient increases for higher void fractions, with a discrepancy at a void fraction of about 10%. It was shown that this deviation is also related to the maximum number of bubbles that can coordinate themselves in a horizontal plane. The effects of preferential horizontal alignment on the averaged drag experienced by the bubbles may need to be taken into account explicitly in drag closure correlations.

ACKNOWLEDGEMENTS

This work is part of the research programme of the Foundation for Fundamental Research on Matter (FOM), which is financially supported by the Netherlands Organisation for Scientific Research (NWO).

REFERENCES

- ALEXANDER, ROGER. 1977. Diagonally Implicit Runge-Kutta Methods for Stiff O.D.E.'s. *SIAM Journal on Numerical Analysis*, **14**(6), 1006–1021.
- BUNNER, B., & TRYGGVASON, G. 2002. Dynamics of homogeneous bubbly flows Part I. Rise velocity and microstructure of the bubbles. *Journal of Fluid Mechanics*, **466**, 17–52.
- DEEN, N. G., VAN SINT ANNALAND, M., & KUIPERS, J. A. M. 2004. Multi-scale modeling of dispersed gas-liquid two-phase flow. *Chemical Engineering Science*, **59**(8-9), 1853–1861.
- DIJKHUIZEN, WOUTER. 2008. *Derivation of closures for bubbly flows using Direct Numerical Simulations*. Ph.D. thesis, University of Twente.
- FRANCOIS, MARIANNE M., CUMMINS, SHAREN J., DENDY, EDWARD D., KOTHE, DOUGLAS B., SICILIAN, JAMES M., & WILLIAMS, MATTHEW W. 2006. A balanced-force algorithm for continuous and sharp interfacial surface tension models within a volume tracking framework. *Journal of Computational Physics*, **213**(1), 141–173.
- FRENKEL, DAAN, & SMIT, BEREND. 2002. Monte Carlo Simulations. Pages 23–61 of: *Understanding Molecular Simulation (Second Edition)*, second edition edn. San Diego: Academic Press.
- HUA, JINSONG, STENE, JAN F., & LIN, PING. 2008. Numerical simulation of 3D bubbles rising in viscous liquids using a front tracking method. *Journal of Computational Physics*, **227**(6), 3358–3382.
- KAUSCH, H. H., FESKO, D. G., & TSCHOEGL, N. W. 1971. The Random Packing of Circles in a Plane. *Journal of Colloid and Interface Science*, **37**(3), 603–611.
- LOCKETT, M. J., & KIRKPATRICK, R. D. 1975. Ideal bubble flow and actual flow in bubble columns. *Transactions of the Institution of Chemical Engineers*, **53**, 267–273.
- MEI, R., LAWRENCE, C. J., & KLAUSNER, J. F. 1994. A note on the history force on a spherical bubble at finite Reynolds number. *Phys. Fl.*, **6**, 418–420.
- PROSPERETTI, A. 2002. Navier-Stokes numerical algorithms for free-surface flow computations: an overview. *Drop-surface interaction*, **237**.
- RENARDY, YURIKO, & RENARDY, MICHAEL. 2002. PROST: A Parabolic Reconstruction of Surface Tension for the Volume-of-Fluid Method. *Journal of Computational Physics*, **183**(2), 400–421.
- RICHARDSON, J.F., & ZAKI, W.N. 1954. Sedimentation and fluidisation: Part I. *Transactions of the Institution of Chemical Engineers*, **32**(Supplement 1), 35–53.
- SIMONNET, M., GENTRIC, C., OLMOS, E., & MIDOUX, N. 2007. Experimental determination of the drag coefficient in a swarm of bubbles. *Chemical Engineering Science*, **62**, 858–866.
- SINGH, R., & SHYY, W. 2007. Three-dimensional adaptive Cartesian grid method with conservative, interface restructuring and reconstruction. *J. Comp. Ph.*, **224**, 150–167.
- TOMIYAMA, A., KATAOKA, I., ZUN, I., & SAKAGUCHI, T. 1998. Drag Coefficients of Single Air bubbles under normal and micro gravity conditions. *JSME Int. J. Series B*, **41**, 472–479.
- UNVERDI, S. O., & TRYGGVASON, G. 1992. A front tracking method for viscous, incompressible, multi-fluid flows. *J. Comp. Ph.*, **100**, 25.
- VAN SINT ANNALAND, M., DIJKHUIZEN, W., DEEN, N. G., & KUIPERS, J. A. M. 2006. Numerical simulation of gas bubbles behaviour using a 3D front tracking method. *AIChE J.*, **52**, 99–110.